High gain, large area, and solar blind avalanche photodiodes based on Al-rich AlGaN grown on AlN substrates

Cite as: Appl. Phys. Lett. 116, 081101 (2020); https://doi.org/10.1063/1.5138127 Submitted: 13 November 2019 . Accepted: 09 February 2020 . Published Online: 24 February 2020

Pramod Reddy 🗓, M. Hayden Breckenridge 🗓, Qiang Guo 🗓, Andrew Klump 🗓, Dolar Khachariya, Spyridon Pavlidis, Will Mecouch 🗓, Seiji Mita, Baxter Moody, James Tweedie, Ronny Kirste, Erhard Kohn, Ramon Collazo, and Zlatko Sitar (1)











High gain, large area, and solar blind avalanche photodiodes based on Al-rich AlGaN grown on AlN substrates

Cite as: Appl. Phys. Lett. **116**, 081101 (2020); doi: 10.1063/1.5138127 Submitted: 13 November 2019 · Accepted: 9 February 2020 · Published Online: 24 February 2020







Pramod Reddy,^{1,a)} D M. Hayden Breckenridge,² D Qiang Guo,² D Andrew Klump,² D Dolar Khachariya,³
Spyridon Pavlidis,³ Will Mecouch,¹ D Seiji Mita,¹ Baxter Moody,¹ James Tweedie,¹ Ronny Kirste,¹ Erhard Kohn,²
Ramon Collazo,² and Zlatko Sitar^{1,2} D

AFFILIATIONS

Adroit Materials, Inc., 2054 Kildaire Farm Rd., Cary, North Carolina 27518, USA

ABSTRACT

We demonstrate large area (25 000 μ m²) Al-rich AlGaN-based avalanche photodiodes (APDs) grown on single crystal AlN substrates operating with differential (the difference in photocurrent and dark current) signal gain of 100 000 at 90 pW ($<1~\mu$ W cm²) illumination with very low dark currents <0.1 pA at room temperature under ambient light. The high gain in large area AlGaN APDs is attributed to a high breakdown voltage at 340 V, corresponding to very high breakdown fields \sim 9 MV cm² as a consequence of low threading and screw dislocation densities $<10^3$ cm². The maximum charge collection efficiency of 30% was determined at 255 nm, corresponding to the bandgap of Al_{0.65}Ga_{0.35}N, with a response of 0.06 A/W. No response was detected for $\lambda >$ 280 nm, establishing solar blindness of the device.

Published under license by AIP Publishing. https://doi.org/10.1063/1.5138127

Compact and efficient avalanche photodiodes (APDs) capable of robust and rugged operation at room and elevated temperatures while being sensitive only in the deep-UV regime with ambient/ visible light rejection capabilities are of great interest for new technology and applications in biological and chemical compound detection, UV-based light detection, ranging [light detection and ranging (LIDAR)] and imaging, radiation detection, etc. A key advantage Al_xGa_{1-x}N has over other materials, such as SiC and GaN, is that for x > 0.45, AlGaN exhibits solar blindness, which renders no response for $\lambda > 290$ nm (AM1.5). Furthermore, the expected minority carrier densities and hence the dark current in AlGaN are extremely low, even at elevated temperatures, with Al_{0.65}Ga_{0.35}N exhibiting a similar dark current density at 1300 K as Si at 300 K. In addition, theoretical analysis of the band structure indicates unlikely hole ionization in $Al_xGa_{1-x}N$ with x > 0.6 opening possibilities of high single carrier multiplication with high gain in linear regime and low noise factors.^{2,3} Hence, AlGaN-based APDs are expected to be solar blind, highly sensitive, smaller, less expensive, and more robust than current UV detectors. Several groups have fabricated APDs on Al_xGa_{1-x}N (x > 0.4) grown on foreign (sapphire) substrates; however, these

devices were either limited in area (700 μ m²) for a gain of 12 000 or in gain (<5500) when the device area was increased up to \sim 8000 μ m^{2,4–7} Consequently, an interesting trend in decreasing gain and efficiency may be inferred with increasing APD size. We hypothesize that large screw dislocation densities are likely the cause of this limited performance of avalanche breakdown devices for larger area devices based on AlGaN on sapphire, as is observed in GaN.⁸⁻¹¹ Hence, in this work, we demonstrate that APDs with AlGaN grown on single crystal PVT AlN substrates with threading dislocation density $(TDD) < 10^3 \,\mathrm{cm}^{-2}$ (compared with typical TDD in the range from 10⁹ cm⁻² to 10¹⁰ cm⁻² when grown on sapphire)¹²⁻¹⁵ result in a significant performance gain even for APDs with significantly larger size. Due to significant challenges arising with poor Ohmic contacts and low conductivity (DX formation and compensation) at Al compositions x > 0.8, Al composition in the range from $x \sim 0.65$ to ~ 0.75 has been employed in the APD structure. ^{16–19} In the fabricated APDs, we have demonstrated a high gain of \sim 100 000 in devices that are 25 000 μ m² in size, with a low bias leakage (dark) current < 0.1 pA and a low voltage external quantum efficiency of 0.3 for unity gain.

²Department of Materials Science and Engineering, North Carolina State University, Raleigh, North Carolina 27695-7919, USA

³Department of Electrical and Computer Engineering, North Carolina State University, Raleigh, North Carolina 27695-7919, USA

a) Author to whom correspondence should be addressed: preddy@ncsu.edu

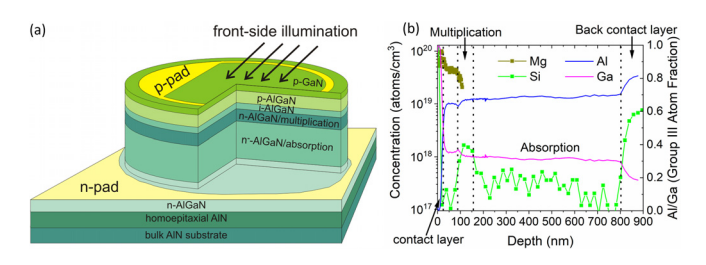


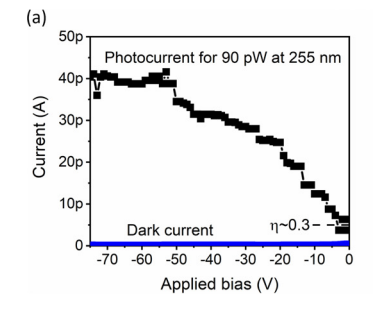
FIG. 1. (a) A schematic of the fabricated APDs and (b) SIMS analysis showing the Mg and Si doping and Al/Ga composition of all the layers of the APD.

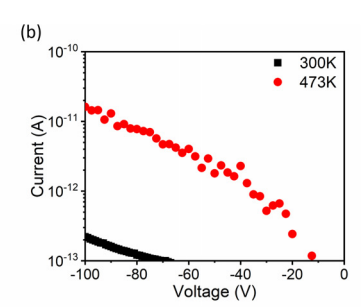
The phenomena that influence the APD design are Mg memory or carry forward in metalorganic chemical vapor deposition (MOCVD) growth of III-nitrides; ^{20,21} compensating defects (C_N , vacancy oxygen complexes, and threading dislocations), which provide the low doping limit in AlGaN π (absorption) region; ^{22–26} dislocation mediated leakage; ^{8,9,27} poor contacts to p-AlGaN; and absorbing AlN substrates in the UVC region (<265 nm). ²²

APD structures (25 000 μ m²) were grown on AlN single crystal substrates in a vertical, rf-heated low-pressure, cold wall MOCVD reactor. To avoid the Mg memory effects, the APD structure terminated with Mg-doped p-AlGaN and a p-GaN contact layer grown under V/III = 2000 under H₂ diluent. Point defect compensators in the low doped absorption region are controlled to $\leq 10^{17} \,\mathrm{cm}^{-3}$ by chemical potential control (where the formation energies of the compensating defects are increased by tuning the metal and nitrogen chemical potentials in the growth environment and this requires intermediate N richness by V/III = 2250 under H_2 diluent). For high conductivity, n-AlGaN contact layer was grown under more N poor (V/III = 700) conditions. 19 TDD-related compensation 12,29 and dislocation mediated leakage is practically negligible when grown on single crystal AlN with $TDD < 10^3 \text{ cm}^{-3}.14,\overline{15},\overline{50}$ Further details of the growth, epitaxy quality, and composition measurement techniques are provided elsewhere. 12,19,31-33 Hence, APD is designed as a hole multiplication device with the absorption region serving as a charge separation region, providing only holes toward the multiplication region. Since screw dislocations have been demonstrated to be a source of leakage in gallium nitride p-n junctions, 8,9 employing foreign substrates such as sapphire resulting in threading dislocation densities >10¹⁰ cm⁻², which may only be reduced to a still significant and deleterious $\sim 10^9 \,\mathrm{cm}^{-2}$ by employing various methods of dislocation reduction, 34-37 is not sufficient to achieve high performance APDs. TDD-related compensation 12,29 and dislocation mediated leakage is practically negligible when grown on single crystal AlN with TDD $<10^3\,\rm cm^{-2}\,^{14,15,30}$

The thickness of the " π " region, where most of the photon absorption occurs, was 500 nm, which is thick enough for >99% of light absorption. The p-n multiplication region was designed to be 50 nm/50 nm with a doping of $2 \times 10^{18} \text{ cm}^{-3}$ in n and $2 \times 10^{19} \text{ cm}^{-3}$ in p with a narrow (~10 nm) undoped i-region between the doped layers. Finally, a thin p-GaN ([Mg] \sim 2 × 10¹⁹ cm⁻³) layer was employed as a contact layer. APDs were fabricated on insulating AIN substrates consisting of a quasi-vertical structure with mesa-etched, beveled (~20°) sidewalls. V/Al/Ni/Au-based Ohmic contact metallization scheme was used for the n-contact, 16,38,39 and the contact anneal was performed using rapid thermal anneal (RTA) at 850 $^{\circ}$ C for 1 min under N_2 ambient. Due to absorption in AlN substrates, ^{22,40–42} the APD was designed for front illumination. Ni/Au Ohmic contact rings were deposited on p-GaN, and the contact was annealed at 600 °C for 10 min in air ambient. 43 Device fabrication was realized with a laser lithography process and a chlorinebased ICP-RIE. Contact metallization included e-beam evaporation and lift-off processes. A schematic of the fabricated AlGaN APD is shown in Fig. 1(a). The thicknesses, composition, and doping of different layers were verified by SIMS and are shown in Fig. 1(b).

We identify the key APD performance metrics for operation in the deep UV regime as (a) room temperature operation, (b) solar blindness and ambient light rejection capability, (c) low dark current, and (d) high gain. Accordingly, we characterized the fabricated APDs at room temperature under dark and illuminated conditions with ambient room lighting and white LEDs. The characterized APDs demonstrate an excellent ambient light rejection capability with no perceivable increase in the reverse current under illumination either by white LED array or by room lighting. The low bias dark current (I_d) was observed to be <0.1 pA (the ammeter limit) shown in Fig. 2(a). The dark current increases at high reverse bias, shown in Fig. 2(b), indicating the single carrier multiplication in Al-rich AlGaN, which was theoretically predicted by Bellotti and Bertazzi² in Al-rich (x > 0.6) Al_xGa_{1-x}N and is corroborated by the strongly temperature activated dark current [Fig. 2(b)]. It has been shown previously that hexagonal hillock features seen after AlGaN epitaxy on AlN substrates originate from threading dislocations in AlN. 44 Since the density of hillocks was comparable with the TDD at $\sim 10^3 \, \text{cm}^{-2}$, the devices with hillocks exhibited threading dislocations and those without hillocks had a high chance of not exhibiting threading dislocations. Since hillocks are visible, they allow the characterization of the influence of threading





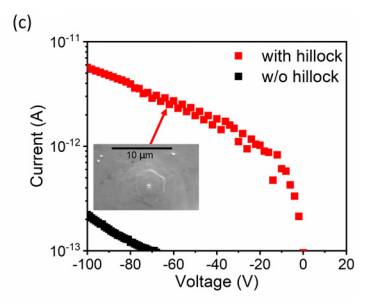


FIG. 2. (a) The dark and photocurrent (for $\lambda=250$ nm) for Al_{0.65}Ga_{0.35}N-based APD (25 000 μm^2), (b) the temperature dependence of dark current, and (c) the impact of hillock (or threading dislocations) on the dark current.

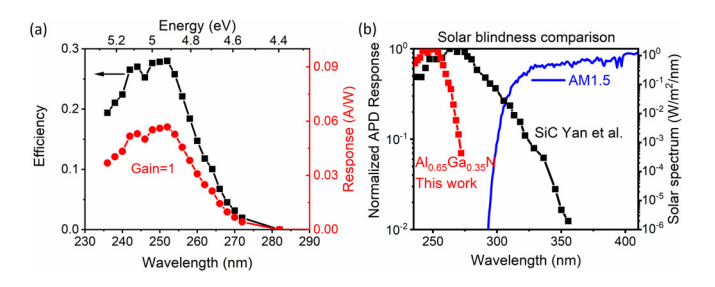


FIG. 3. The charge collection quantum efficiency and response as a function of wavelength. (b) A comparison of normalized spectral response of $AI_{0.65}Ga_{0.35}N$ - and SiC-based (Ref. 45) APDs with the solar spectrum (Reference AM1.5 spectra from ASTMG173-03 tables).

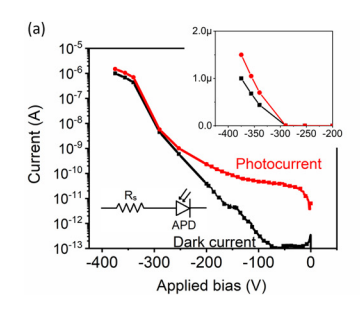
dislocations. Figure 2(c) shows reverse characteristics for devices with and without hillocks and consequently with and without threading dislocations. It is clear that threading dislocations increase the reverse leakage and hence dark current and results in poor APD performance, and it supports our hypothesis that threading dislocations were responsible for the limited performance of APDs on sapphire. The APDs were then characterized under illumination using a xenon lamp attached to a monochromator for wavelength selection. Under illumination, there is a clear increase in the reverse current relative to the dark current, as shown in Fig. 2(a), where the illumination was at 255 nm and 90 pW of incident optical power. From the photocurrent (Ip) and known intensity of light as a function of wavelength at low bias (<5 V), the charge collection quantum efficiency (η) was determined as a function of wavelength for the APD. As expected for a direct bandgap semiconductor with a bandgap of 4.9 eV (Al_{0.65}Ga_{0.35}N), the efficiency was maximum at 4.9 eV ($\lambda = 255$ nm) at $\sim 30\%$, corresponding to a response of \sim 0.06 A/W. The spectral dependence of the efficiency and response are shown in Fig. 3(a). As will be discussed later in this work, efficiency increases with the increase in reverse bias, and the reported efficiency is the "low bias" efficiency. Further, efficiency is lowered due to the thin region of absorbing p-GaN contact layer in the top-illuminated APD where \sim 40% of the incident optical power is absorbed. The absorption in the \sim 25 nm of p-GaN layer was estimated using Beer-Lambert law from an absorption coefficient of $\sim 2 \times 10^5$ cm⁻¹ at wavelength of interest (\sim 250 nm). This reduced the efficiency by \sim 20%. The APD response [Fig. 3(a)] was found to be immeasurable for $\lambda > 280$ nm. Hence, the solar blind rejection ratio (R_{255 nm}/R_{280 nm}) and UV/visible rejection ratio ($R_{255\,\mathrm{nm}}/R_{400\,\mathrm{nm}}$) is >1800 and > 12000, respectively, assuming that the visible and 280 nm response are lower than measurement noise in the dark current. Further, the solar blindness of the APD is apparent from Fig. 3(b) showing the APD response and solar spectrum; SiC APD response is included for comparison (from Ref. 45).

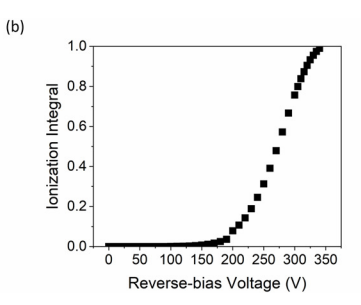
We finally characterized the ionization gain of the APD. The illumination was at 255 nm and 90 pW of incident optical power. The dark and photocurrents are shown in Fig. 4(a). Note that the current is limited in the μ A range by a protection circuit involving a series resistor. The gain is high at voltages >340 V, when the current is limited by the series resistance with technology computer-aided design (TCAD) simulations with ATLAS framework by Silvaco, indicating corresponding parallel plane fields ~9 MVcm⁻¹. Further, TCAD simulations predicting the ionization integral employing the ionization coefficients predicted by Bellotti and Bertazzi for Al_{0.6}Ga_{0.4}N [ionization coefficient for electrons is $6 \times 10^8 (\text{cm}^{-1}) \exp(-6 \times 10^7 \text{ MV cm}^{-1}/\text{E})$, and for holes, it is relatively low $2 \times 10^5 (\text{cm}^{-1}) \exp(-3 \times 10^7 \text{ MV cm}^{-1}/\text{E})$ where E is the applied electric field] resulted in a breakdown voltage of \sim 340 V in reasonably good agreement with our experimental results indicating the importance of high quality (low threading dislocation density) epitaxy for achieving the theoretical limits of the nitride system. The ionization integral is shown in Fig. 4(b) as a function of applied

The difference between dark and photocurrent is defined as APD signal and is plotted in Fig. 4(c). The similarity in the signal function and photocurrent indicates an ionization gain that modulates any current flowing through the device. The gain is defined as 46

Gain =
$$\frac{I_p(V) - I_d(V)}{I_p(V_0) - I_d(V_0)}$$
, (1)

where V_0 is the reverse voltage, where gain is 1 (assumed for <5 V) and is shown in Fig. 4(c). We report a maximum gain of ~100 000 at an input power of 90 pW (<1 μ W cm⁻²). Further, the breakdown voltage exhibited a positive temperature coefficient of ~0.04 V/K as shown in Fig. 5(a) confirming the avalanche nature of breakdown. It must be noted that the unity gain photocurrent, where the efficiency is calculated and employed as a reference for calculation of gain, is not clearly defined and varies in literature. Increasing the reverse bias extends the depletion region into the absorption region producing the electric fields required to separate the generated electron-hole pairs. Hence, efficiency increases with increased reverse bias. However, ionization gain may also be introduced, resulting in overestimation of





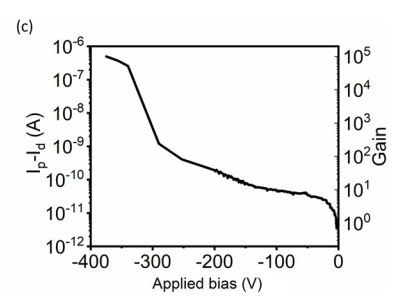
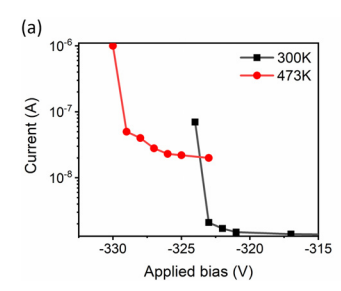


FIG. 4. (a) Photocurrent (at 250 nm) and Dark current under reverse bias conditions in the tested APD structure. The left inset shows the circuit diagram with series protection resistance and the right inset shows the current in a linear scale. (b) The simulated ionization integral as a function of applied reverse bias. (c) The APD signal (difference in the dark and photocurrent) and the corresponding signal gain.



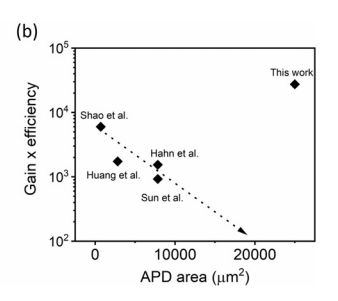


FIG. 5. (a) The avalanche breakdown region as a function of temperature. (b) A comparison of FOM obtained in this work on AlGaN grown on AlN single crystalline substrates with those obtained on AlGaN grown on sapphire as a function of APD area as reported in the literature. 4–7.

efficiency albeit with an underestimation of gain. Consequently, the product of gain and efficiency as a figure of merit (FOM) representing the ratio of electrons or holes collected per unit time to the number of photons incident per unit time is employed to provide a better comparison among the different groups. The maximum FOM was calculated to be $\sim 30\,000$. Note that in this case, the gain was limited by a series protection resistance [circuit diagram is shown in inset in Fig. 4(a)] with higher currents resulting in a destructive breakdown. Finally, a compilation of FOMs from reported gain and efficiencies by different groups on $A_{lx}Ga_{1-x}N$ APDs with x>0.4 is shown in Fig. 5(b). It is clear that the combination of point defect and dislocation density management results in vastly improved performance even for large area APDs necessary for practical applications.

We have demonstrated Al-rich AlGaN-based avalanche photodiodes (APDs) grown on single crystal AlN substrates operating with a maximum signal gain of 100 000 at 90 pW (<1 μ W cm $^{-2}$) with very low dark currents (<0.1 pA) at room temperature under ambient light. The high gain is attributed to the high breakdown voltage of 340 V, corresponding to very high breakdown fields $>9\,\mathrm{MVcm}^{-1}$ as a consequence of a low threading and screw dislocation densities $<10^3\,\mathrm{cm}^{-2}$. The maximum charge collection efficiency of $\sim\!30\%$ was determined at 255 nm, corresponding to the bandgap of Al $_{0.65}\mathrm{Ga}_{0.35}\mathrm{N}$, with a response of 0.06 A/W. Further, no response was detected for $\lambda > 280\,\mathrm{nm}$, establishing the solar blindness requirement.

The authors acknowledge the funding in part from PNNL (No. NA-22-WMS-66204), AFOSR (No. FA9550-17-1-0225), NSF (Nos. ECCS-1508854, ECCS-1653383, and ECCS-1916800), and ARO (Nos. W911NF-15-2-0068, W911NF-16-C-0101, W911NF-18-1-0415, and W911NF-14-C-0008).

REFERENCES

- ¹G. A. Shaw, A. M. Siegel, J. Model, A. Geboff, S. Soloviev, A. Vert, and P. Sandvik, Proc. SPIE 7320, 73200J (2009).
- ²E. Bellotti and F. Bertazzi, J. Appl. Phys. 111, 103711 (2012).
- ³E. Bellotti and F. Bertazzi, Proc. SPIE **8980**, 89800R (2014).
- ⁴L. Hahn, F. Fuchs, L. Kirste, R. Driad, F. Rutz, T. Passow, K. Köhler, R. Rehm, and O. Ambacher, Appl. Phys. Lett. 112, 151102 (2018).
- ⁵Y. Huang, D. J. Chen, H. Lu, K. X. Dong, R. Zhang, Y. D. Zheng, L. Li, and Z. H. Li, Appl. Phys. Lett. **101**, 253516 (2012).

- ⁶Z. G. Shao, D. J. Chen, H. Lu, R. Zhang, D. P. Cao, W. J. Luo, Y. D. Zheng, L. Li, and Z. H. Li, IEEE Electron Device Lett. **35**, 372 (2014).
- ⁷L. Sun, J. Chen, J. Li, and H. Jiang, Appl. Phys. Lett. **97**, 191103 (2010).
- ⁸J. W. P. Hsu, M. J. Manfra, R. J. Molnar, B. Heying, and J. S. Speck, Appl. Phys. Lett. 81, 79 (2002).
- ⁹S. Usami, Y. Ando, A. Tanaka, K. Nagamatsu, M. Deki, M. Kushimoto, S. Nitta, Y. Honda, H. Amano, Y. Sugawara, Y.-Z. Yao, and Y. Ishikawa, Appl. Phys. Lett. 112, 182106 (2018).
- 10 A. Chatterjee, S. K. Khamari, V. K. Dixit, S. M. Oak, and T. K. Sharma, J. Appl. Phys. 118, 175703 (2015).
- ¹¹Y. Saitoh, K. Sumiyoshi, M. Okada, T. Horii, T. Miyazaki, H. Shiomi, M. Ueno, K. Katayama, M. Kiyama, and T. Nakamura, Appl. Phys. Express 3, 081001 (2010)
- ¹²I. Bryan, Z. Bryan, S. Washiyama, P. Reddy, B. Gaddy, B. Sarkar, M. Hayden Breckenridge, Q. Guo, M. Bobea, J. Tweedie, S. Mita, D. Irving, R. Collazo, and Z. Sitar, Appl. Phys. Lett. 112, 062102 (2018).
- ¹³R. Dalmau, B. Moody, R. Schlesser, S. Mita, J. Xie, M. Feneberg, B. Neuschl, K. Thonke, R. Collazo, A. Rice, J. Tweedie, and Z. Sitar, J. Electrochem. Soc. 158, H530 (2011).
- ¹⁴D. Ehrentraut and Z. Sitar, MRS Bull. 34, 259 (2009).
- ¹⁵R. Dalmau and Z. Sitar, in *Springer Handbook of Crystal Growth*, edited by G. Dhanaraj, K. Byrappa, V. Prasad, and M. Dudley (Springer, Berlin/Heidelberg, 2010), pp. 821–843.
- ¹⁶R. France, T. Xu, P. Chen, R. Chandrasekaran, and T. D. Moustakas, Appl. Phys. Lett. **90**, 062115 (2007).
- ¹⁷R. Collazo, S. Mita, J. Xie, A. Rice, J. Tweedie, R. Dalmau, and Z. Sitar, Phys. Status Solidi C 8, 2031 (2011).
- ¹⁸L. Gordon, J. L. Lyons, A. Janotti, and C. G. Van de Walle, Phys. Rev. B 89, 085204 (2014).
- ¹⁹P. Reddy, Q. Guo, J. Tweedie, S. Washiyama, F. Kaess, S. Mita, M. H. Breckenridge, R. Kirste, R. Collazo, A. Klump, B. Sarkar, and Z. Sitar, in IEEE Research and Applications of Photonics in Defense (RAPID) Conference (2018), pp. 1–4.
- ²⁰A. Agarwal, M. Tahhan, T. Mates, S. Keller, and U. Mishra, J. Appl. Phys. **121**, 025106 (2017).
- ²¹H. Xing, D. S. Green, H. Yu, T. Mates, P. Kozodoy, S. Keller, S. P. DenBaars, and U. K. Mishra, Jpn. J. Appl. Phys., Part 1 42, 50 (2003).
- ²²D. Alden, J. S. Harris, Z. Bryan, J. N. Baker, P. Reddy, S. Mita, G. Callsen, A. Hoffmann, D. L. Irving, R. Collazo, and Z. Sitar, Phys. Rev. Appl. 9, 054036 (2018).
- 23S. G. Christenson, W. Xie, Y. Y. Sun, and S. B. Zhang, J. Appl. Phys. 118, 135708 (2015).
- ²⁴D. O. Demchenko, I. C. Diallo, and M. A. Reshchikov, Phys. Rev. Lett. 110, 087404 (2013).
- 25 F. Kaess, S. Mita, J. Xie, P. Reddy, A. Klump, L. H. Hernandez-Balderrama, S. Washiyama, A. Franke, R. Kirste, A. Hoffmann, R. Collazo, and Z. Sitar, J. Appl. Phys. 120, 105701 (2016).
- ²⁶J. L. Lyons, A. Janotti, and C. G. V. de Walle, Appl. Phys. Lett. 97, 152108 (2010).
- ²⁷J. S. Speck and S. J. Rosner, Physica B **273–274**, 24 (1999).
- ²⁸P. Reddy, S. Washiyama, F. Kaess, R. Kirste, S. Mita, R. Collazo, and Z. Sitar, J. Appl. Phys. **122**, 245702 (2017).
- 29 E. C. H. Kyle, S. W. Kaun, P. G. Burke, F. Wu, Y.-R. Wu, and J. S. Speck, J. Appl. Phys. 115, 193702 (2014).
- 30 R. Schlesser, R. Dalmau, and Z. Sitar, J. Cryst. Growth 241, 416 (2002).
- ³¹J. Tweedie, R. Collazo, A. Rice, J. Xie, S. Mita, R. Dalmau, and Z. Sitar, J. Appl. Phys. **108**, 043526 (2010).
- ³²I. Bryan, Z. Bryan, S. Mita, A. Rice, L. Hussey, C. Shelton, J. Tweedie, J.-P. Maria, R. Collazo, and Z. Sitar, J. Cryst. Growth 451, 65 (2016).
- ³³R. Kirste, Q. Guo, J. H. Dycus, A. Franke, S. Mita, B. Sarkar, P. Reddy, J. M. LeBeau, R. Collazo, and Z. Sitar, Appl. Phys. Express 11, 082101 (2018).
- ³⁴D.-S. Wuu, H.-W. Wu, S.-T. Chen, T.-Y. Tsai, X. Zheng, and R.-H. Horng, J. Cryst. Growth 311, 3063 (2009).
- 35M. J. Kappers, R. Datta, R. A. Oliver, F. D. G. Rayment, M. E. Vickers, and C. J. Humphreys, J. Cryst. Growth 300, 70 (2007).
- 36 S. Sakai, T. Wang, Y. Morishima, and Y. Naoi, J. Cryst. Growth 221, 334 (2000)

- ³⁷S. Keller, B. P. Keller, Y.-F. Wu, B. Heying, D. Kapolnek, J. S. Speck, U. K. Mishra, and S. P. DenBaars, Appl. Phys. Lett. 68, 1525 (1996).
- ³⁸B. B. Haidet, B. Sarkar, P. Reddy, I. Bryan, Z. Bryan, R. Kirste, R. Collazo, and Z. Sitar, Jpn. J. Appl. Phys., Part 1 56, 100302 (2017).
- J. O. Song, S. H. Kim, J. S. Kwak, and T. Y. Seong, Appl. Phys. Lett. 83, 1154 (2003).
 R. Collazo, J. Xie, B. E. Gaddy, Z. Bryan, R. Kirste, M. Hoffmann, R. Dalmau, B. Moody, Y. Kumagai, T. Nagashima, Y. Kubota, T. Kinoshita, A. Koukitu, D. L. Irving, and Z. Sitar, Appl. Phys. Lett. 100, 191914 (2012).
- ⁴¹Q. Yan, A. Janotti, M. Scheffler, and C. G. Van de Walle, Appl. Phys. Lett. 105, 111104 (2014).
- ⁴²B. E. Gaddy, Z. Bryan, I. Bryan, J. Xie, R. Dalmau, B. Moody, Y. Kumagai, T. Nagashima, Y. Kubota, T. Kinoshita, A. Koukitu, R. Kirste, Z. Sitar, R. Collazo, and D. L. Irving, Appl. Phys. Lett. 104, 202106 (2014).
- 43B. Sarkar, P. Reddy, A. Klump, F. Kaess, R. Rounds, R. Kirste, S. Mita, E. Kohn, R. Collazo, and Z. Sitar, J. Electron. Mater. 47, 305 (2018).
- ⁴⁴Z. Zhang, M. Kushimoto, T. Sakai, N. Sugiyama, L. J. Schowalter, C. Sasaoka, and H. Amano, Appl. Phys. Express 12, 124003 (2019).
- ⁴⁵F. Yan, J. H. Zhao, and G. H. Olsen, Solid-State Electron 44, 341 (2000).
- ⁴⁶D. Decoster and J. Harari, *Optoelectronic Sensors*, 1 ed. (Wiley/ISTE, Hoboken, NJ/London, 2009).